Molecular Simulation of Adsorption in Microporous Materials

M. Yiannourakou, P. Ungerer, B. Leblanc, X. Rozanska, P. Saxe, S. Vidal-Gilbert, F. Gouth, F. Montel

Photos: Corbis, DOI: 10.2516/ogst/2012104, IFPEN, X.

Dossier

This paper is a part of the hereunder thematic dossier published in OGST Journal, Vol. 68, No. 6, pp. 951-1113 and available online here

Cet article fait partie du dossier thématique ci-dessous publié dans la revue OGST, Vol. 68, n°6, pp. 951-1113 et téléchargeable ici

DOSSIER Edited by/Sous la direction de : **C. Barrère-Tricca**

IFP Energies nouvelles International Conference / Les Rencontres Scientifiques d'IFP Energies nouvelles

MAPI 2012: Multiscale Approaches for Process Innovation

MAPI 2012 : Approches multi-échelles pour l'innovation des procédés

Oil & Gas Science and Technology – Rev. IFP Energies nouvelles, Vol. 68 (2013), No. 6, pp. 951-1113

Oil & Gas Science and Technology – Rev. IFP Energies nouvelles, Vol. 68 (2013), No. 6, pp. 977-994

DOI: 10.2516/ogst/2013134

IFP Energies nouvelles International Conference
Rencontres Scientifiques d'IFP Energies nouvelles

MAPI 2012: Multiscale Approaches for Process Innovation
MAPI 2012 : Approches multi-échelles pour l'innovation des procédés

Molecular Simulation of Adsorption in Microporous Materials

M. Yiannourakou[1]*, P. Ungerer[1], B. Leblanc[1], X. Rozanska[1], P. Saxe[2], S. Vidal-Gilbert[3], F. Gouth[3] and F. Montel[3]

[1] *Materials Design Sarl, 18 Rue de Saisset, 92120 Montrouge - France*
[2] *Materials Design Inc., 6 First National Place, Angel Fire, NM 87710 - USA*
[3] *Total - CSTJF, 26 avenue Larribau, 64000 Pau - France*
e-mail: myiannourakou@materialsdesign.com

* Corresponding author

Résumé — **Modélisation moléculaire de l'adsorption dans les solides microporeux** — L'existence de logiciels industriels, la baisse du coût du calcul et la disponibilité de champs de force éprouvés rendent la simulation moléculaire de plus en plus attrayante pour les applications du domaine du génie chimique. Nous présentons ici plusieurs applications des techniques de simulation de Monte-Carlo, appliquées à l'adsorption de fluides dans des solides microporeux (pores < 2 nm) comme les zéolithes et des structures microporeuses à base de carbone. L'adsorption a été modélisée par simulation dans l'ensemble Grand Canonique grâce au logiciel MedeA®-GIBBS, en utilisant des grilles tridimensionnelles de valeurs pré-calculées de l'énergie pour optimiser le temps calcul. MedeA®-GIBBS a aussi été utilisé pour obtenir les potentiels chimiques ou les fugacités dans les phases fluides libres au moyen de l'ensemble Canonique (NVT) ou de l'ensemble isotherme-isobare (NPT). Les résultats de simulation ont été comparés avec des données expérimentales d'isothermes d'adsorption de corps purs (gaz hydrocarbures, eau, aromatiques, éthanethiol) dans plusieurs zéolithes et à plusieurs températures. La coadsorption de mélanges (méthane-éthane, *n*-hexane-benzène) dans les zéolithes a aussi été étudiée. Par exemple, l'inversion de sélectivité *n*-hexane/benzène entre la silicalite et les Na-faujasites est bien prédite avec des champs de force publiés, et permettent de comprendre les mécanismes sous-jacents. De même, les isothermes d'adsorption des hydrocarbures légers et d'un mercaptan (éthyl-thiol) sont bien décrite. En ce qui concerne les adsorbants organiques (kérogène et charbons matures), des modèles moléculaires moyens ont été construits en rendant compte des principaux traits connus de la structure chimique de ces matériaux. Par une simple relaxation à base de dynamique moléculaire, nous avons pu obtenir des densités moyennes en bon accord avec les données expérimentales disponibles, ce qui est très encourageant. Nous avons aussi déterminé les courbes isothermes d'excès d'adsorption en bon accord qualitatif avec celles récemment mesurées sur des échantillons de charbon ou d'argiles en l'absence d'eau. Bien que préliminaires, ces résultats illustrent la puissance et la généralité de la modélisation moléculaire en vue de la compréhension de systèmes complexes dans des conditions où l'expérimentation est difficile.

Abstract — ***Molecular Simulation of Adsorption in Microporous Materials*** — *The development of industrial software, the decreasing cost of computing time, and the availability of well-tested*

forcefields make molecular simulation increasingly attractive for chemical engineers. We present here several applications of Monte-Carlo simulation techniques, applied to the adsorption of fluids in microporous solids such as zeolites and model carbons (pores < 2 nm). Adsorption was computed in the Grand Canonical ensemble with the MedeA®-GIBBS software, using energy grids to decrease computing time. MedeA®-GIBBS has been used for simulations in the NVT or NPT ensembles to obtain the density and fugacities of fluid phases. Simulation results are compared with experimental pure component isotherms in zeolites (hydrocarbon gases, water, alkanes, aromatics, ethanethiol, etc.), and mixtures (methane-ethane, n*-hexane-benzene), over a large range of temperatures. Hexane/benzene selectivity inversions between silicalite and Na-faujasites are well predicted with published forcefields, providing an insight on the underlying mechanisms. Also, the adsorption isotherms in Na-faujasites for light gases or ethane-thiol are well described. Regarding organic adsorbents, models of mature kerogen or coal were built in agreement with known chemistry of these systems. Obtaining realistic kerogen densities with the simple relaxation approach considered here is encouraging for the investigation of other organic systems. Computing excess sorption curves in qualitative agreement with those recently measured on dry samples of gas shale is also favorable. Although still preliminary, such applications illustrate the strength of molecular modeling in understanding complex systems in conditions where experiments are difficult.*

INTRODUCTION

Adsorption processes are important in chemical engineering: separation of aromatic isomers, drying, removal of VOC (Volatile Organic Chemicals) from air or industrial gases, hydrogen separation from flue gas, oxygen separation from air, are largely based on the properties of industrial adsorbents to adsorb selectively key compounds that would not separate efficiently by distillation. Zeolites and activated carbons are often used for this purpose, because of their high selectivity and stability in regeneration conditions [1]. More recently, metal-organic frameworks have extended the range of possible adsorbents with a considerable array of possible combinations. However, the implementation of adsorption processes in the industry is often limited by the cost and delay of experimental data acquisition, and by the lack of simple methods for predicting adsorption properties.

In this context, several factors make molecular modeling increasingly attractive for industrial applications: the availability of powerful algorithms for complex systems, the development of industrial software allowing efficient use by chemical engineers, the decreasing cost of computing time, and the parameterization of well-tested forcefields.

The purpose of the present article is to illustrate this trend in the case of Monte-Carlo and Molecular Dynamics simulation techniques, applied to the adsorption of fluids in microporous solids such as zeolites and model carbons. The work is mostly oriented towards microporous materials (pores < 2 nm).

Section 1 of the article is devoted to the methods: forcefields, statistical ensembles, sampling dynamics and equilibrium properties, and post-processing in the MedeA® environment.

Section 2 is devoted to application examples in which we compare the simulated behavior as much as possible with experimental data.

In Section 3 we discuss the benefits and limitations of current implementations from an industrial point of view. This will comprise adsorption of alkanes, aromatics and thiols in zeolites, water adsorption in single wall carbon nanotubes, and adsorption of methane and water in gas shales. Although the organic matter in gas shales is not specifically an industrial adsorbent, its study is typical of the insight provided by molecular level modeling, in a context where the exact structure is not known. This insight is particularly useful for the oil and gas industry, as the adsorption of natural gas in kerogen is considered to play a significant role during the depletion of gas shales [2, 3].

In Section 3, we summarise the conclusions and perspectives of this study, based on the discussion presented on each application example of Section 2.

1 METHODS

1.1 Monte-Carlo Simulation of Adsorption Equilibrium

The number of adsorbed molecules in a microporous solid is classically obtained by a simulation in the Grand Canonical ensemble [4], where the imposed parameters

are the chemical potential(s) μ_i of the adsorbed molecular type(s), temperature T and volume V. The adsorbent is considered as rigid, so that there is no need to consider solid-solid interaction energy. As we will consider high pressure gases, it is convenient to impose component fugacities f_i, which is equivalent to impose chemical potentials. Both variables are related by:

$$\mu_i = \mu_{io} + RT \ln\left(\frac{f_i}{f_{io}}\right) \quad (1)$$

The advantage of imposing fugacity is that it reduces to partial pressure in the limit of low pressure:

$$\lim_{P\to 0} \frac{f_i}{Py_i} = 1 \quad (2)$$

where P is bulk gas pressure and y_i is the molar fraction of component i in the gas phase. A convenient reference state for f_{io}, which is used in MedeA®-GIBBS, is the pure ideal gas under a pressure of 1 Pa at the same temperature.

Care must be taken that the principle of Grand Canonical Monte-Carlo (GCMC) is thermodynamic equilibrium, and it does not account for possible kinetic limitations. This is generally a desirable advantage of Monte-Carlo methods for sampling all possible adsorption sites in complex microporous solids. However, the case of unconnected micropores or "bottleneck" micropores makes GCMC results delicate to interpret. We will see in Section 2.2 an example illustrating this point.

1.2 Molecular Dynamics

Molecular dynamics is mostly used for two purposes in the present study:

– relaxing the structure of carbon-based amorphous solids, for which the detailed structure is known on a statistical basis only;
– accessing the dynamics of gas molecules in the microporosity of the solid.

In both cases, the dynamics depends on the motion of the atoms of the solid, *inter alia*. Appropriate thermostat and barostat have to be used to scale velocities at regular time intervals if temperature T and pressure P are imposed. It must be stressed that the bulk gas pressure P in Equation (2) and the barostat pressure are formally independent, as the barostat pressure acts also on the solid.

In the MedeA® software environment, we are using LAMMPS (large scale atomic massively parallel software) for molecular dynamics simulations [5].

1.3 ForceFields

In this work, we call Forcefield a homogeneous set of rules and parameterizations that is used to describe intermolecular forces and intermolecular potential energy.

In molecular dynamics, we use mainly the following all-atoms forcefields:

1. the Polymer Consistent ForceField (PCFF) forcefield was the result of research conducted by the biosym potential energy functions and polymer consortia (mostly between 1989 and 2004) [6]. Their consistent use of Quantum Mechanics (QM) for parameterization generally results in a high quality representation of intra-molecular valence interactions (bond stretching, angle bending, torsion etc.). Since 2009, refined and extended PCFF (PCFF+) [7] is being developed at *Materials Design, Inc*. in order to correct this limitation, and it is only PCFF+ that makes extensive use of experimental liquid densities and cohesive energy/heat of vaporization in the parameterization of the non-bonds (PCFF used mostly crystal data to estimate Lennard-Jones (LJ) parameters). A specific combining rule is used for Lennard-Jones interactions between unlike atoms in PCFF and PCFF+;
2. the Optimized Potentials for Liquid Simulations forcefield (All Atom) (OPLS-AA) forcefield developed by Jorgensen *et al*. [8], based on a Lennard-Jones (LJ) 6-12 for non-bond interactions and a geometric combining rule for each parameter. The geometric combining rule is used in OPLS-AA to get the Lennard-Jones interaction parameters between unlike force centers.

Both forcefields use partial charges located on atomic nuclei and Coulomb's law of electrostatics to get intermolecular interactions. Appropriate terms are introduced in OPLS-AA and in PCFF to treat intramolecular interactions between atoms separated by one bond (stretching), two bonds (bending) or three bonds (torsion). Intra-molecular electrostatics and Lennard-Jones interactions are considered between atoms separated by more than 3 bonds.

When using Monte-Carlo techniques, we used mainly United Atoms (UA) forcefields, which make simulations less demanding in computing time because the hydrogens atoms are not considered explicitly. The Transferable Potentials for Phase Equilibria forcefield (TraPPE) parameterization of this model by the group of Siepmann [9-13] has been used, as well as the Anisotropic United Atoms (AUA) description [14, 15] with optimized parameters for hydrocarbons and functionalized compounds [16-24]. Both AUA and UA models use constant bond lengths. They use the same torsion and bending terms as Optimized Potentials for Liquid

Simulations forcefield (United Atom) (OPLS-UA), which was limited to hydrocarbons.

In applying forcefield to complex systems (either multicomponent mixtures or multifunctional carbonaceous solids), the assignment of the appropriate forcefield parameters would be very long and error-prone if not automated. A significant part of forcefield implementation in the MedeA® software environment has been devoted to the development and testing of appropriate rules for selecting forcefield types and assigning partial charges to atoms, stretching types to bonds and all other forcefield parameters.

1.4 Energy Calculation

When the solid is assumed rigid in Grand Canonical simulations, the solid-solid interaction energy is constant, and its contribution to the system energy may be neglected. This allows to deal with numerous microporous solids [4].

When the location of the cations may change in the simulation of faujasites, the variations of solid-cation interaction energy (electrostatic + repulsion + dispersion) are considered, in addition to cation-adsorbate energy [25, 26].

1.5 Statistical Bias and Configurational Bias

A good sampling is delicate to achieve when simulating the adsorption of gases or volatile liquids in microporous solids. This may be explained by the dense packing of molecules in narrow pores.

Configurational Bias Monte-Carlo (CBMC) [27, 28] is used in MedeA®-GIBBS to build or grow linear and branched molecules that may exhibit several conformations. This bias speeds up the exploration of the configurational space that would be otherwise impossible in narrow channels [29]. Concerted rotations (flip, CONROT) are implemented to explore the possible conformations of inner parts of linear chains [30]. These moves are implemented in accordance with microscopic reversibility [31, 32] so that the statistical ensemble is correctly sampled.

In the case of cyclic or branched molecules, a canonical reservoir bias technique [18, 33, 34] is used to speed up the sampling of new conformations.

1.6 Computational Details

1.6.1 Grids in GCMC

The potential energy of interaction between the sorbed molecules and the adsorbent is pre-calculated over a finely-meshed grid that is overlaid on the simulation unit-cell. In this approach, the adsorbent is treated as a rigid body, its atoms having no freedom of movement, which speeds-up the calculation.

1.6.2 Number of Unit Cells

The simulation box may consist of one or more unit-cells. The use of the unit cell for the energy grid(s) calculation and the replication of this grid in space, allows the use of considerably smaller files in the simulation than if the energy grid(s) were calculated on the entire simulation box. Linear interpolation between the nearest 8 nodes of the grid is used to determine energy in a given location.

1.6.3 Calculation of Electrostatic Interactions

The fluid-fluid electrostatic interactions are treated, depending on the forcefield used, with Ewald summation or cutoff and addition of long-range corrections.

The grid of solid-fluid electrostatic interactions may be computed by two classes of methods:

- using point electrostatic charges on framework atoms, and computing the relevant interaction with a unit charge on each node with Ewald summation. Partial charges such as those proposed by Uytterhoven *et al.* [35], Mortier *et al.* [36] may be used. In zeolites, this method allows to treat Al and Si as *T* atoms with partial charges, which avoids to make explicit assumptions on the location of Al sites;
- using a Vienna Ab initio Simulation Package (VASP) calculation to compute directly the electrostatic potential created by the framework atoms on each node of the grid [37]. This original method takes advantage of the theoretical basis of *ab-initio* quantum chemistry, but requires to specify explicitly the identity of each atom (such as Al and Si atoms in cation-exchanged zeolites). This presents the advantage that the solid structure may be optimized before grid generation, providing thus a way to check its consistency before starting GCMC calculations. As the GCMC calculation is able to consider supercells without increasing the size of the electrostatic grid file, this method provides a way to benefit from a large part of the exactness of quantum simulations when computing adsorption equilibria. In many cases, the computing time required by the VASP calculation is not larger than the computing time required to perform the GCMC calculations involved in an isotherm. The method allows thus a fairly efficient multiscale calculation offering the best of quantum- and forcefield-based methods.

1.6.4 Monte-Carlo Moves, Frequencies

The following moves are available in MedeA®-GIBBS for adsorption studies:

- molecular insertions and deletions with pre-insertion bias using either rotational bias [38] for rigid molecules, CBMC for linear and branched molecules, and reservoir bias for cyclic molecules (*Sect. 1.5*);
- translation of a molecule, considered as a rigid body [31];
- rotation of a molecule, considered as a rigid body [31];
- CBMC regrowth of a chain (*Sect. 1.5*);
- reptation move, *i.e.* suppressing *m* atoms at one end of a chain and adding *m* atoms at the other end, using configurational bias to generate and select the new configuration;
- flip move, *i.e.* rotation of an inner atom in a chain or in a flexible cycle around the axis of its two immediate neighbors);
- pivot move (rotation of a part of a molecule around a pivot atom);
- CONROT move, *i.e.* concerted motion of several successive atoms in a linear chain [30];
- swap move, *i.e.* exchange of a simple molecule (LJ particle + charge) by a molecule of another type;
- displacement of a simple molecule (LJ particle + charge), *i.e.* translation to a randomly selected location and biased regrowth.

In addition to these moves, the following moves are available in the NPT ensemble to simulate bulk fluid phases:

- volume change [31];
- Widom test insertions [39] to determine chemical potential and fugacity of selected molecular types. This move is implemented with the same statistical bias as molecular insertions in the Grand Canonical ensemble.

As microscopic reversibility is satisfied, the probability density of the ensemble does not depend on the frequency of the above Monte-Carlo moves, with one condition: each possible degree of freedom must be sampled [31].

When simulating multi-component systems, defining the frequency of each Monte-Carlo move for each compound would be long if not helped by the software environment. For this reason, default frequencies are proposed by MedeA®-GIBBS to sample all relevant degrees of freedom. This analysis is also providing an educated guess of the minimum number of Monte-Carlo steps to provide meaningful averages.

The reference state (fugacity $f_{io} = 1$ Pa, at the same temperature) does not depend on the parameters of statistical bias such as the number of test positions to grow the chain by one atom [40]. As a consequence, partial pressures may be used instead of fugacities in Grand Canonical simulations if the microporous solid is in thermodynamic equilibrium with an ideal vapor phase. This is generally the case for gases below 1 bar with a good approximation.

1.7 MedeA® Environment

A variety of different tools is employed to facilitate the study of sorption of various molecules onto different solid structures. These tools include crystal structure databases, adsorption and desorption options and a graphical way of setting up simulation protocols, post-processing of results, visualization and analysis of the results.

1.7.1 Crystal Structure Databases and Symmetry Space Groups

Crystal structure databases (ICSD, NCD, Pearson, Pauling) are available in MedeA® through a search engine that accepts multiple criteria, providing an efficient way of searching among numerous different structure(s) which best fit a specific study or research area of interest, editing and manipulating the structure(s) at will and finally creating the solid that will be used as the simulation adsorbent.

1.7.2 Adsorption Isotherms, Detection of Hysteresis

Hysteresis loops during adsorption and desorption of gases in micro-and mesoporous materials have been repeatedly reported in literature [41] and related to differences in adsorption/desorption mechanisms, swelling phenomena and relaxation of sorbed molecules clusters inside the micropores. Molecular simulations have been proven to be extremely valuable in studying the mechanisms of adsorption and desorption into pores of different sizes and provide insight on the hysteresis observed [42-44].

1.7.3 Flowcharts

A very important part of experimental research relies on building and using specific protocols, based on the systems, the properties investigated, and the methods used in the study. Establishing such protocols assures the reproducibility of the results, the minimization of human error introduced in the study and the ability to build on accumulated knowledge throughout the scientific community.

Much in the same sense, such work protocols need to be established for simulation studies. Common practices involve the use of such protocols or computation recipes, as they are often referred to in literature, in each research group. However, not much work has been devoted in appropriate book-keeping of these protocols and communicating them in a consistent and efficient way.

Flowcharts, easily built and saved in MedeA®, target exactly this need. Flowcharts contain all the necessary information for running a simulation under the exact same conditions at any time, while at the same time, having the ability to change any of the simulation parameters and conditions. It is an easy and efficient way of communicating a protocol between researchers with a single file.

1.7.4 Post-Processing: Convergence, Visualization, Analysis

The post-processing or simulation results, is itself an art. It requires a lot of knowledge on the simulation processes and their limitations as well of the systems studied and the properties calculated. Convergence analysis of each property calculated throughout the simulation run, provides an unambiguous way of treating the simulation results.

A unique advantage of molecular simulations is the knowledge of the exact positioning and orientation of the sorbed molecules inside the adsorbent. Visualization of different snapshots of the equilibrated system may reveal nucleation sites, cluster formation, mono- or multilayer adsorption, micro-phase separations, hydrophilic or hydrophobic regions, the energetic or entropic origin of sorption of various compounds on a solid. Combining this knowledge with experimental findings and theoretical scenarios, may reveal the governing factors leading to the macroscopic behavior observed.

Combining visualization with specific location analysis, as for example in the case of the location analysis of cations in a faujasite, provides a way of studying and understanding cation exchange phenomena [45] during waste water treatment.

1.8 Limitations

There are several challenges when dealing with complex systems, areas where there is still much space for improving current methodologies for molecular simulation.

One of these challenges is the transferability of forcefield parameters used for the adsorbents. Currently, there is no unique forcefield that can be used to describe accurately the Van der Waals as well as the electrostatic interactions for a wide range of solids, either organic or inorganic. This issue is magnified when dealing with solids which consist of both organic and inorganic regions, such as Metal Organic Frameworks (MOF). Insight from *ab-initio* studies [37, 46] may help greatly in establishing ways of defining new forcefields that may describe these complex materials, capturing the essence of their chemical behavior. Polarization effects have been introduced [47] but there is still a poor understanding and accounting for those effects in adsorption studies [48].

Molecular Dynamics and Monte-Carlo simulations have been used to study cation location in zeolites [49, 50] and cation exchange [45]. The results show that the utilization of molecular simulation on such systems is very promising and can provide qualitatively and quantitatively accurate description.

2 APPLICATION EXAMPLES

With the application examples presented here, we are aiming at presenting case studies covering a wide range of adsorbents, from highly symmetric structures to amorphous systems, with or without cations present (which in their turn may be considered either immobile or be allowed to move in the solid).

Our effort is aiming at presenting the use of GCMC simulations as a means of predicting and understanding the adsorption of pure compounds as well as multicomponent mixtures by using available knowledge from literature (whenever this is feasible) on the solid structures or using molecular simulation to create realistic structures.

2.1 Adsorption of Alkanes on Silicalite-1

The adsorption of light hydrocarbons in silicalite-1 (MFI or ZSM-5) is a well known system on which several teams have tested forcefield and configurational bias algorithms for equilibrium [51, 52] and dynamic behavior [53]. These studies demonstrated not only the feasibility of performing such simulations but also the quantitative agreement with experimental data. Du *et al.* [51] have obtained adsorption isotherms for methane and alkanes, for a wide range of pressures, and they have compared them with experimental data [54-56]. Their results show an excellent agreement, both qualitatively and quantitatively, with the experimental data, for a wide range of pressures and temperatures, as it can be seen in Figures 1 and 2.

By visualizing the systems, we can also see how the adsorbed molecules accommodate in the zeolite. As it is shown in Figure 3, the alkanes fill the inner part of the channels in silicalite. *n*-butane fills the zeolite channels by aligning parallel to the walls, as do linear alkanes with a higher number of carbon atoms. This behavior is important for understanding the competitive adsorption of alkanes.

Du *et al.* [51] have performed GCMC simulations, to study the adsorption on silicalite-1 of an equimolar mixture of methane and ethane at $T = 250$ K (*Fig. 4*). It can clearly be seen that for the entire pressure range studied, ethane is preferably sorbed on silicalite-1. The sorbed

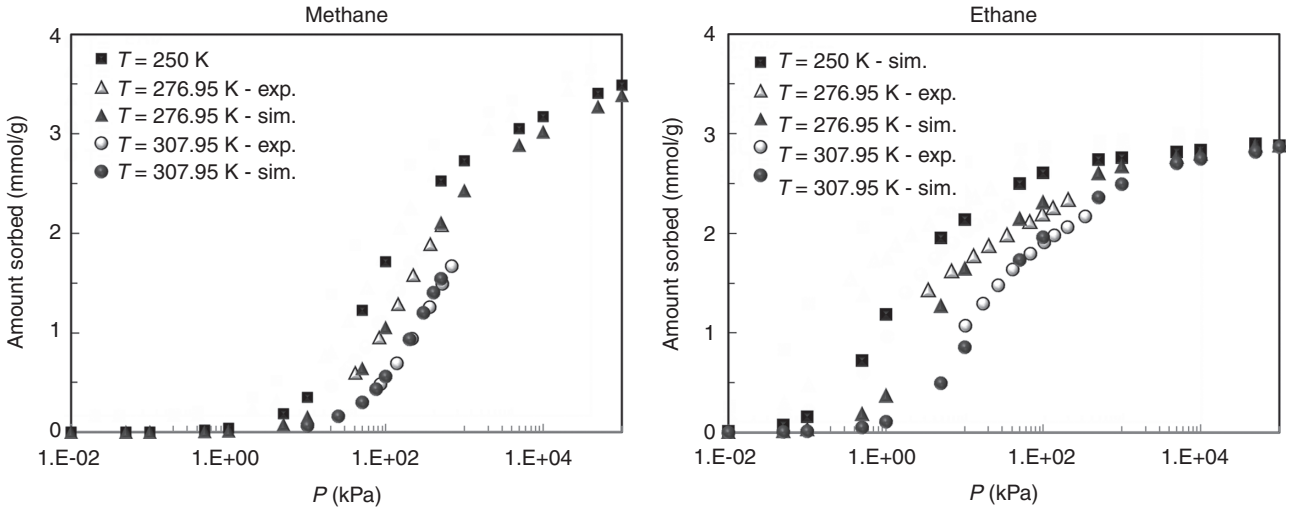

Figure 1

Methane and ethane (TraPPE-UA) adsorption isotherms at different temperatures on MFI zeolite. Open symbols represent experimental data; closed symbols represent simulation results. Reproduction of the simulation work of [51].

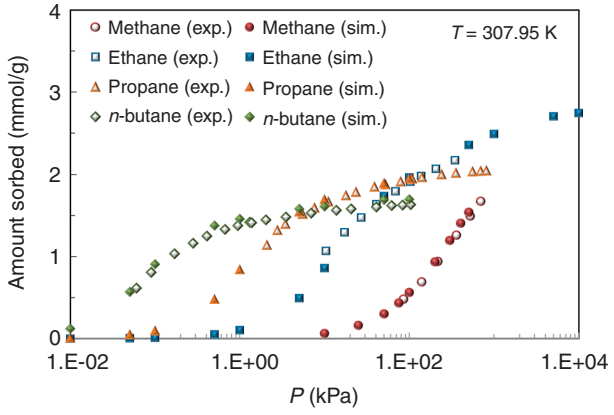

Figure 2

GCMC simulations with MedeA®-GIBBS on MFI zeolite. Comparison with experimental data by Sun *et al.* [55] using TraPPE-UA forcefield for all alkanes.

phase consists almost entirely of ethane at low pressures, while the concentration of methane increases with pressure. Experimentally, Abdul-Rahman *et al.* [56] have observed that, at high pressures, methane tends to replace ethane due to entropic effects.

2.2 Binary Mixture of *n*-hexane/benzene in Silicalite-1

The adsorption of *n*-hexane/benzene liquid mixtures on Silicalite-1 (*Fig. 5*) and Na zeolites (*Fig. 8* in *Sect. 2.3*) has been determined experimentally [57]. These authors have shown that *n*-hexane preferentially adsorbs on silicalite-1. In their experiments, they show that a 4.9% molar concentration of *n*-hexane in the liquid phase leads to 89% (molar concentration) of *n*-hexane in the adsorbed phase. They also observe that the *n*-hexane density in the pores of silicalite-1 is the same as in the bulk liquid, within experimental uncertainty.

We have conducted GCMC simulations for a gas mixture of *n*-hexane/benzene, using the TraPPE forcefield for *n*-hexane and the OPLS-AA model for benzene, at 298.15 K. We observe the same behavior, *i.e.* a marked selectivity for *n*-hexane (*Fig. 6*).

When visualizing the resulting configurations at equilibrium, it is evident that *n*-hexane fills nicely the channel network (straight and zig-zag channels) of silicalite-1, while the few benzene molecules are located on the crossing of the channels where they can better fit (*Fig. 7*). The main reason why benzene does not adsorb in the channels themselves is its larger average diameter. It is likely that the benzene molecules undergo significant kinetic limitations to pass through the channels, especially for high alkane loading. Passing through the channels being a necessary step toward their adsorption sites, equilibration may be sufficiently long that benzene does not adsorb in experiments.

2.3 Binary Mixture of *n*-hexane/benzene in $Na_{48}Y$

Unlike adsorption on Silicalite-1, Yu *et al.* [57] showed experimentally that benzene preferentially adsorbs on

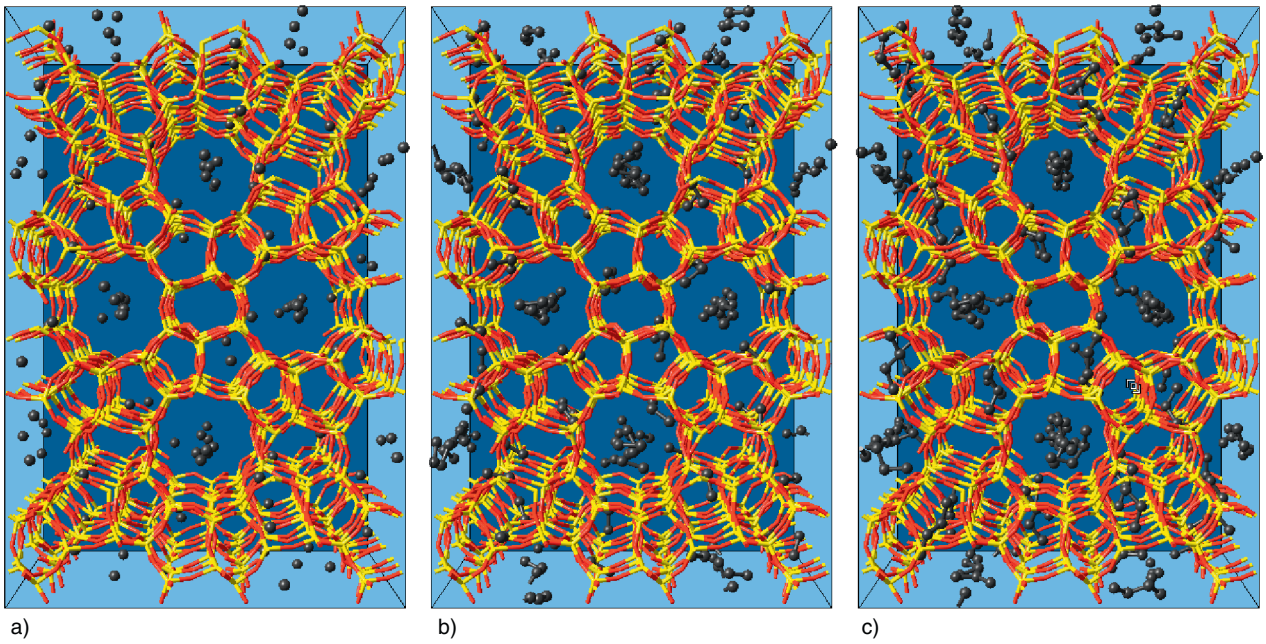

Figure 3

Adsorption on silicalite-1 (MFI) at a high fugacity (high loading), at T = 307.95 K, of pure compounds. a) methane, b) ethane, c) *n*-butane.

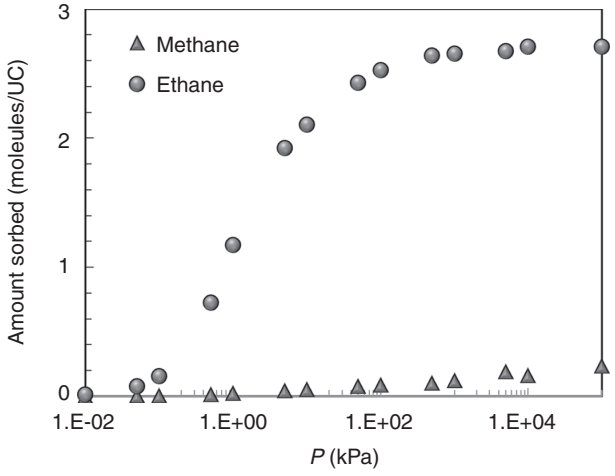

Figure 4

Equimolar binary mixture of CH_4 and C_2H_6 at 250 K. Adsorption in silicalite-1 (MFI). Reproduction of the simulation work of [51].

NaY zeolite in mixtures with *n*-hexane, partly because benzene has a significantly higher saturation loading than *n*-hexane. They show that for low benzene concentrations in the liquid phase, the adsorbed benzene concentration was high (*Fig. 8*).

We performed Grand Canonical simulations of adsorption for a gas mixture of *n*-hexane/benzene, using the TraPPE forcefield (united atom description without electrostatic charges) for *n*-hexane and the OPLS-AA model for benzene (all-atom description with electrostatic point charges on all carbon and hydrogen atoms), at 298.15 K. The OPLS-AA model has been used for benzene, in order to try and capture the essence of the electrostatic profile of the molecule, which is rather important for the case of sorption on faujasite, which contains cations and where electrostatic interactions are deemed to be important in the system's behavior. Si and Al atoms have been treated as undifferentiated T-atoms, and partial electrostatic charges have been allocated according to the prescription of Uytterhoven *et al.* [35]. The experimentally observed selectivity (*Fig. 8*) for benzene is well predicted by our simulations (*Fig. 9*).

As shown in Figure 10, benzene molecules are not randomly distributed in the micropores of faujasites. Further examination shows that they occupy preferentially four sites per supercage, facing the site II cations. This location is pointing out the cause of the selectivity *versus* *n*-hexane: the cation charge interacts favorably with the quadrupole moment of benzene, while *n*-hexane does not display sufficient electrostatic moments to interact so strongly. Also, the three-dimensional network of supercages in silicalite is connected through larger windows

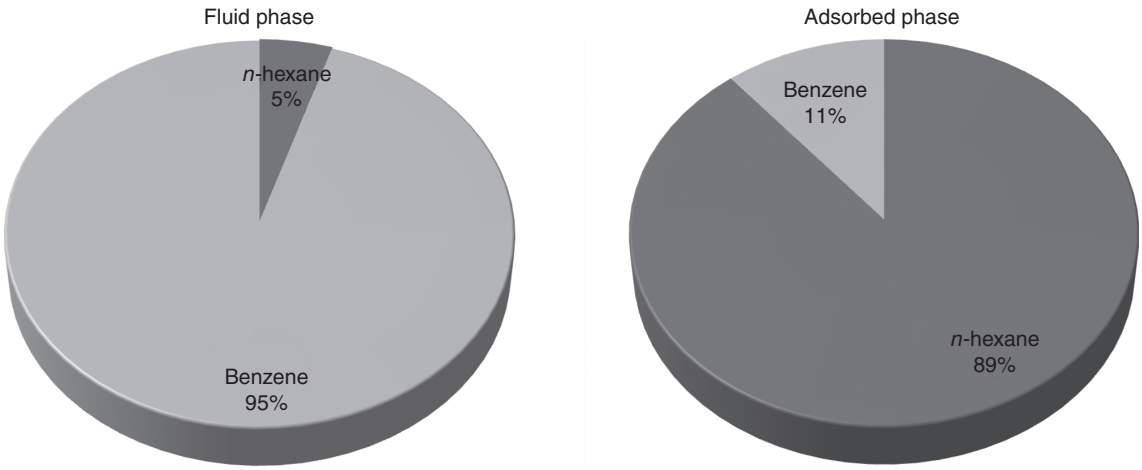

Figure 5

Experimental data for adsorption equilibrium of binary mixtures of *n*-hexane and benzene in silicalite at 295 K.

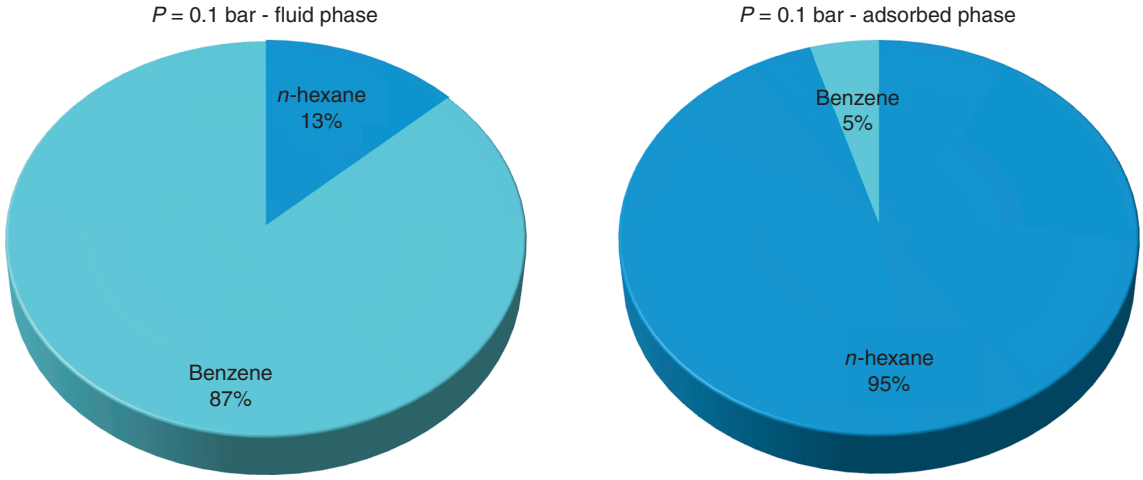

Figure 6

Simulation results from GCMC simulations of binary mixtures of *n*-hexane and benzene in silicalite at a total pressure of 0.1 bar, at 298.15 K.

than the channels of silicalite, so that benzene is not disadvantaged by its large disk shape.

2.4 Ethyl Mercaptan in NaX Faujasite

Ethyl mercaptan (or ethanethiol) is an example of the minor components of natural gas on which severe specifications must be respected to distribute the gas. As its concentration is usually very low (a few ppm), purification by selective adsorption of ethanethiol may be considered for its removal.

The liquid-vapor phase behavior of organic thiols has been investigated in detail with the AUA model [21]. This model has been simplified with a reduced number of electrostatic charges. A simple prescription based on the Lorentz Berthelot combining rule [52] is used for the Lennard-Jones part. The electrostatic part of the energy is described by point charges on T-atoms, according to the prescription of Uytterhoven *et al.* [35].

It is found that this predictive model is in good agreement with the experimental isotherms of ethanethiol in NaX, that have been gathered by Weber *et al.* [58]. The influence of temperature and fugacity, as well as the total capacity of approximately 6 molecules per supercage, are well captured (*Fig. 11*) by this simple model.

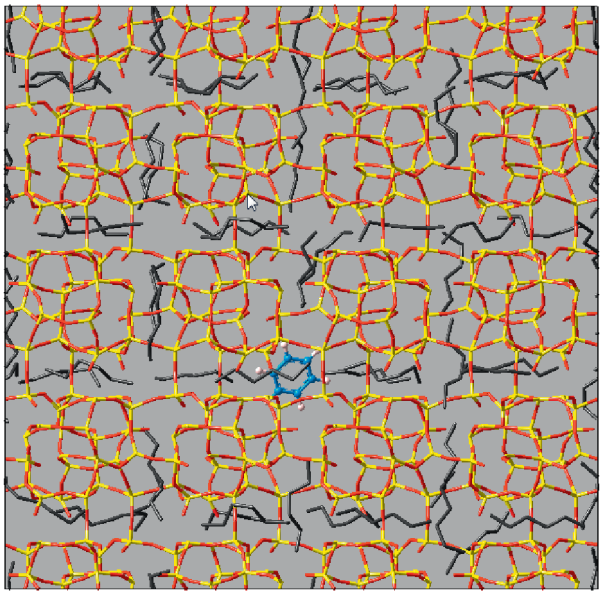

Figure 7

Adsorption of *n*-hexane/benzene mixture on silicalite-1 at 298.15 K.

2.5 Adsorption in Carbon Nanotubes

The small dimensions, strength and the remarkable physical properties of carbon nanotubes make them a very unique material with a whole range of promising applications in nanotechnology, electronics, optics and other fields of materials science and technology, while the whole range of their physical properties is still being discovered and disputed.

Carbon nanotubes may differ in length, diameter, chirality and number of nested tubes. Depending on these characteristics, they may present a wide range of properties.

Their naming depends on the number of nested tubes (*i.e.* single walled/double or multi walled) followed by two numbers which define the precise way in which a graphene sheet is rolled up in order to build the corresponding carbon nanotube chirality, *i.e.* one out of the three distinct ways in which they can be rolled: armchair, zigzag and chiral configuration (*Fig. 12*).

The use of a nanotube builder (building tool of MedeA®) allows a rapid and accurate creation of carbon nanotubes, with a complete control over all the building parameters and geometric characteristics.

The length of the sides of the primitive unit cell that may be used for constructing the simulation box and the interaction energy grid(s) is typically a few Angström, rendering the computational effort and time needed for the grid construction very small. Therefore, the computation of a whole isotherm is usually a matter of a few hours.

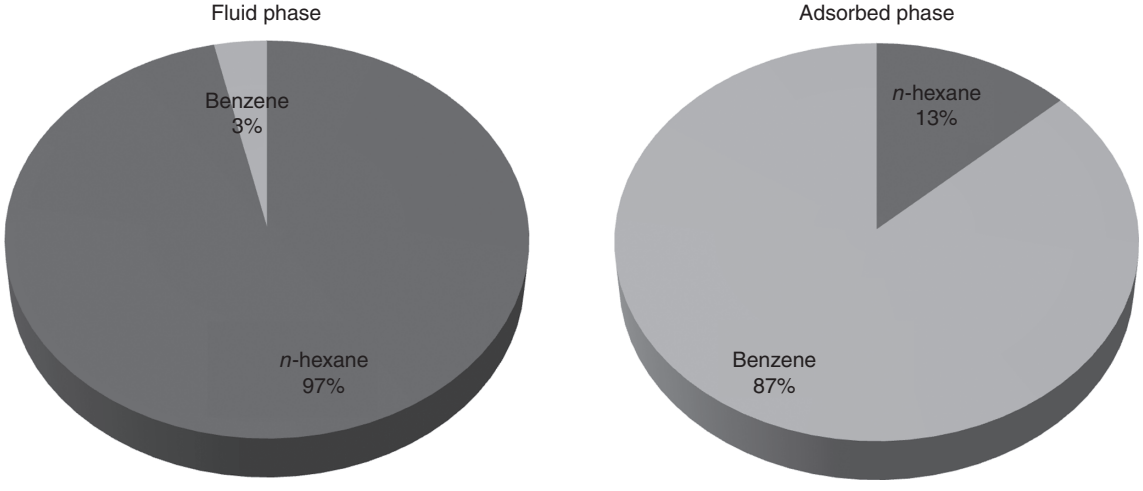

Figure 8

Experimental data [57] for adsorption of binary mixtures of *n*-hexane and benzene in NaY faujasite at 295 K.

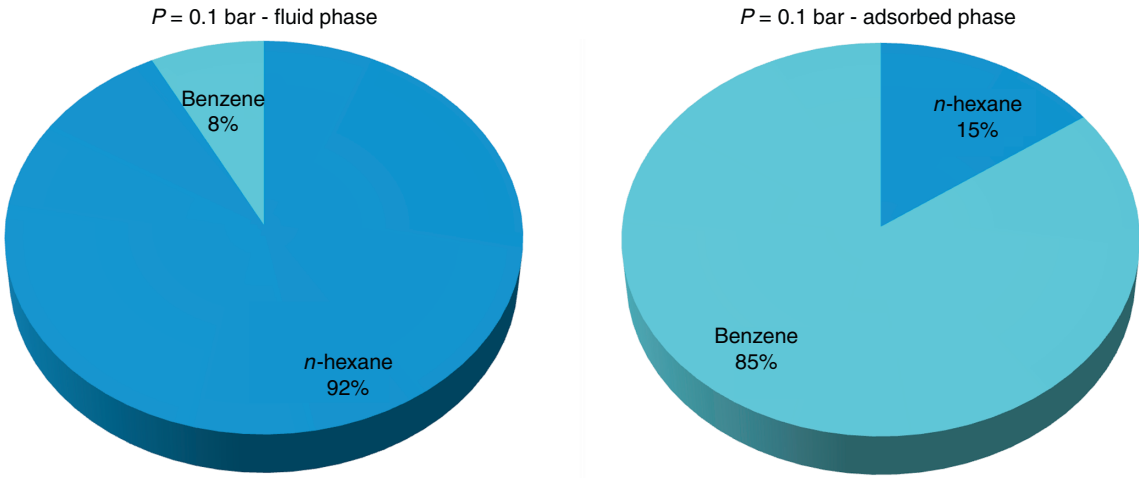

Figure 9

Simulation results from GCMC simulations of binary mixtures of *n*-hexane and benzene in NaY faujasite at a total pressure of 0.1 bar, at 298.15 K.

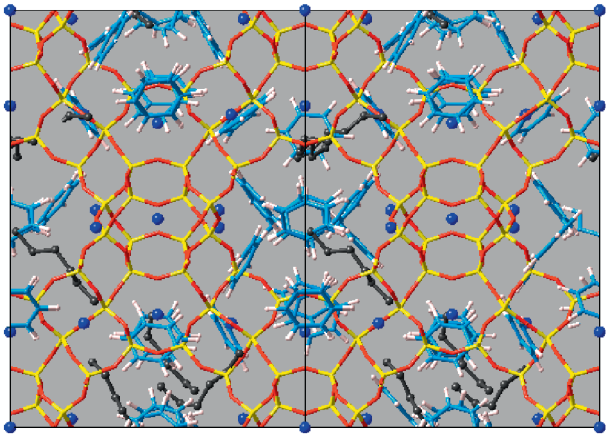

Figure 10

Adsorption of *n*-hexane/benzene mixture on $Na_{48}Y$ at 298.15 K.

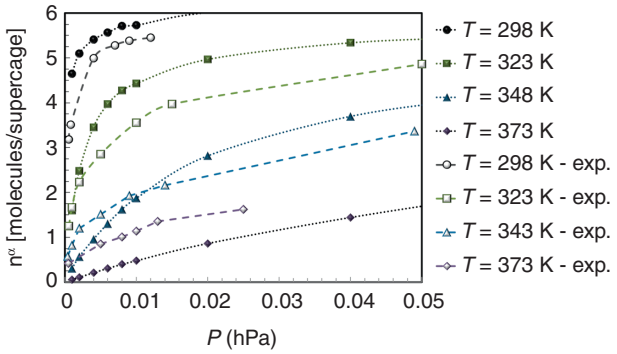

Figure 11

Simulation results and experimental data [58] for adsorption of ethyl mercaptan in $Na_{86}X$. Open symbols are experimental data while filled symbols are simulation results.

On the left hand side of Figure 13, the top view of a simulation box containing single wall carbon nanotubes, with water sorbed at high pressure, is shown, along with the surrounding periodic images of the simulation box. On the right hand side, a small area of a section of a carbon nanotube is shown (at the same temperature and pressure conditions).

A Single Wall Carbon NanoTubes (SWCNT) (11,0) is a narrow nanotube with an internal diameter (C-C distance) of 8.66 Å. Even at very low water fugacities, water is introduced in the nanotube at loadings of approximately 3 $mol \cdot kg^{-1}$ of solid, as it can be seen in Figure 14. Comparing adsorption isotherms at different temperatures, it can be clearly seen how the amount of sorbed water decreases as temperature increases.

2.6 Methane Adsorption in Kerogen

The purpose of this application is to investigate the role of adsorption in the organic micropores of gas shales. As documented in the Barnett formation, an organic-rich

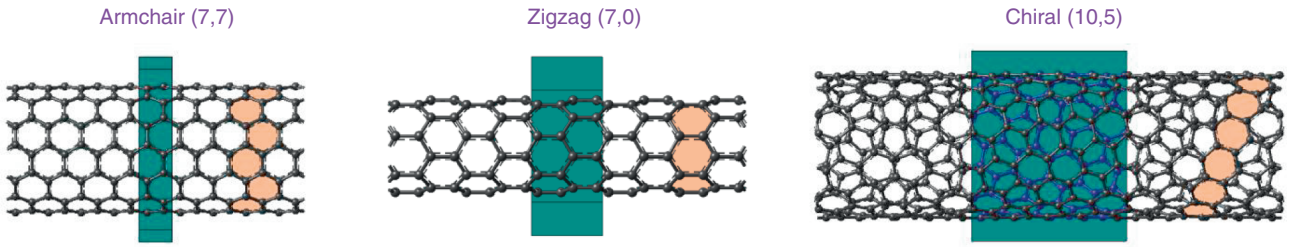

Figure 12

Examples of Single Wall Carbon Nanotubes (SWCNT) with different geometric characteristics. The shaded boxes are the primitive cells of the structures. Many more forms can be built when acting on pitch, spacing, number of nested tubes.

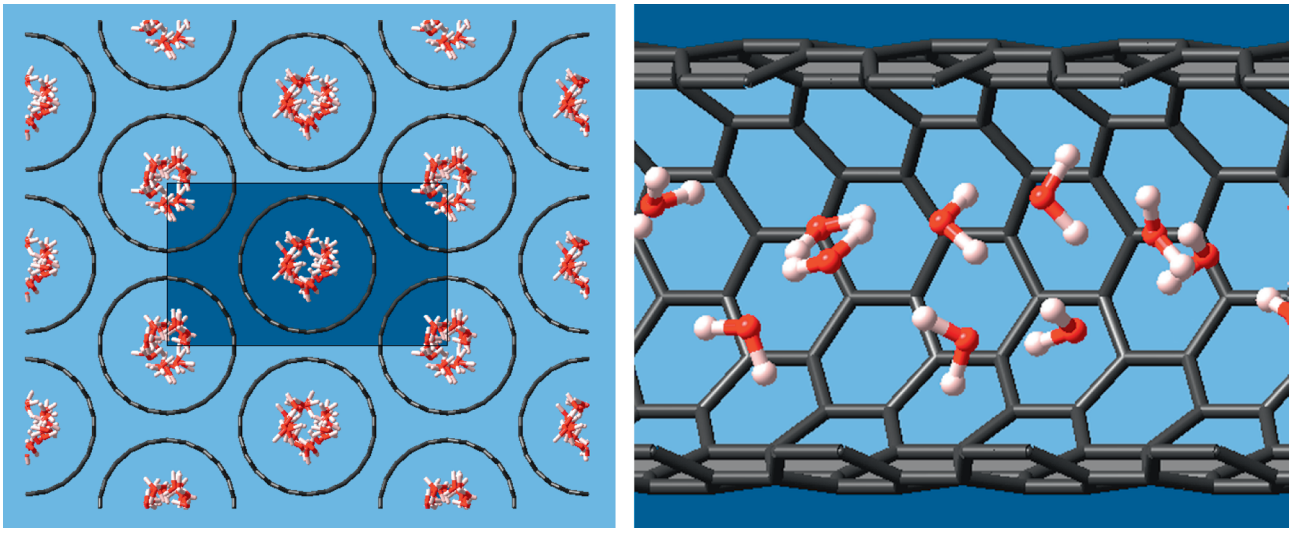

Figure 13

Water adsorption on Single Wall Carbon Nanotubes, at $T = 298$ K. a) Top view of the system surrounded by periodic copies of the simulation box; b) side section view of part of a SWCNT.

shale of Devonian age, shale gas is produced from the same shales in which it has been generated. Detailed analysis by Focused Ion Beam - Scanning Electron Microscope (FIB-SEM) has shown that Barnett shale samples display numerous mesopores (2 to 20 nm) in the organic matter which is a minor, yet significant, component of this gas shale. The present study is focused on mature kerogen, *i.e.* end of oil generation zone/beginning of gas generation zone.

The sedimentary organic matter (or kerogen) that has generated gas in these shales is an aromatic structure with alkyl chains cross-linking polyaromatic units, and numerous functional groups. Much of the chemical structure of kerogen is known from NMR and XPS and related techniques [59]. From this work, an average of 16-20 carbon atoms are involved per polyaromatic cluster in mature kerogen, consistently with a H/C atomic ratio of 0.5 to 0.8. The oxygen content is subordinate (typically O/C = 0.05 to 0.1). Oxygen atoms are mostly present as ether bonds or embedded in aromatic cycles (hydroxyl groups are present in low maturity kerogens but they are no more significant in mature kerogen). Organic sulfur content and nitrogen contents are low (generally N/C $<$ 0.02 and S/C $<$ 0.05 on an atomic basis). The chemical structures containing sulfur and nitrogen in mature kerogen are mostly aromatic cycles (thiophenic, pyrrolic, pyridinic). Amine groups (NH_2, NH) and thiols (-SH) disappear in the early stages of natural maturation. Due to the progressive convergence of kerogen composition and humic coal composition in the late stages of maturation, most of these features apply to mature coals as well. In our kerogen model, we have used all this experimental information to guide building of a model that on average respects the above-

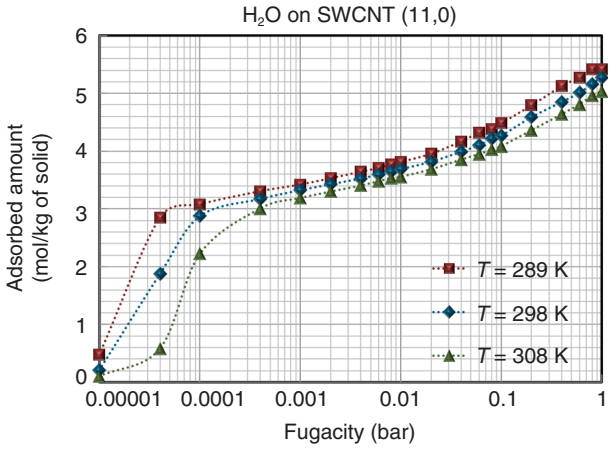

Figure 14

Adsorption isotherms of water in carbon nanotubes.

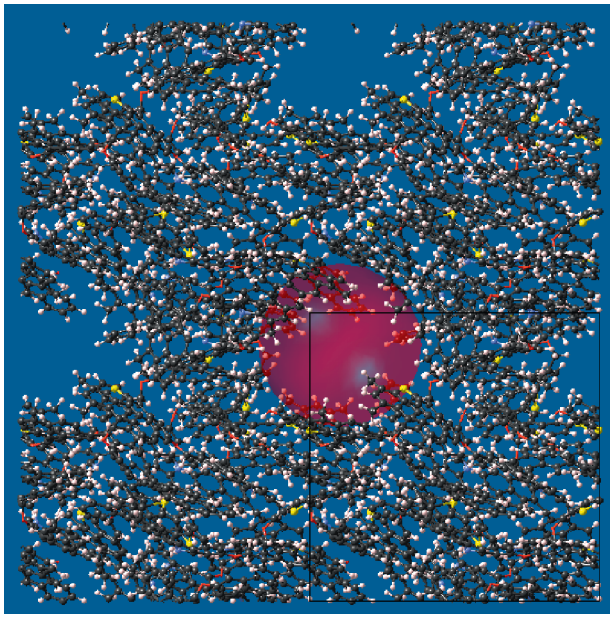

Figure 15

Molecular model of mature kerogen. The line frames the unit cell of the solid (in this view four unit cells are shown). The sphere indicates a nanopore (~1.4 nm width) introduced to simulate qualitatively the presence of pores larger than 1 nm evidenced by FIB-SEM.

mentioned elemental analysis as well as the structural details, of course within a statistical description. It should be noted that no matter how representative a model is, it is still one model, which can by no means provide an exhaustive study of the specific material. To explore in detail the material (kerogen in this case but the same goes for *i.e.* polymers or colloids), a large number of different models should be used and the results should be combined in a meaningful way to provide the complete picture. However, the aim of this study is to provide a set of tools and a protocol that may be followed to study such systems and get information and data that may be directly compared to experimental results. The qualitative and even semi-quantitative agreement that is observed when comparing our simulation results with experimental findings suggests that the model used is able to reproduce the main phenomena that are taking place or even driving the sorption and diffusion in such systems.

The structure is globally amorphous, but some stacking of polyaromatic units is evidenced by electron microscopy [60].

The density of mature kerogen is known to be in the range 1.2 to 1.4 g·cm^{-3} [61] which is a similar range to alginites, the macerals of coal of comparable composition to kerogen [62].

Molecular dynamics was used to build several possible models of mature kerogen, respecting the atomic composition of the organic matter, the percentage of aromatic carbon and the presence of minor groups involving oxygen, sulfur or nitrogen [59]. These models were generated according to the following sequence:

(A) build kerogen "molecules":
- generating polyaromatic fragments with *ab-initio* computed geometries;
- selecting polyaromatic units from the fragment library;
- substitute some carbon atoms by oxygen or sulfur,
- add alkyl groups (mostly methyl) or hydroxyl bonds;
- form kerogen "molecules" by cross-linking 4 polyaromatic units.

(B) relax several kerogen "molecules" by molecular dynamics:
- start from a configuration where each kerogen "molecule" is far away from others;
- perform a molecular dynamics simulation of 1 ns in the NPT ensemble with an imposed temperature, using the PCFF + forcefield.

The molecular weight of the kerogen "molecules" in our models is low (approximately 150 atoms, *i.e.* a molecular mass of approximately 1 000 g·mol^{-1}) compared with accepted values. However, the main purpose here is to generate a structure that can be relaxed. We checked that the above procedure was producing repeatedly kerogen models with the appropriate density (average 1.3 g·cm^{-3} ± 0.05). Average density did not show systematic variations with total pressure or temperature. A significant tendency of polyaromatic units to stack has

been observed in our simulations, in the same way as observed by Zhang and Greenfield in model asphalts [63].

Similarly to coal, kerogen may be considered as a microporous and mesoporous solid where the pores are either due to steric effects (holes between the polyaromatic units) or to local phase split as suggested by FIB-SEM techniques [64]. In order to simulate the behavior of fluids inside large micropores, we imposed an additional dummy particle in the relaxation stage, so that the kerogen model contains a void of approximately spherical shape, 1 nm in diameter, per unit cell (*Fig. 15*). The unit cell is approximately 2.5 nm large. This model allows to model fluids in confined micropores of spherical or tubular shape.

Comparing high pressure sorption isotherms of pure gases from simulations and experiments is made through excess sorption, that is the amount of gas sorbed in the material, minus the amount of gas that would have been present in the pore volume if its density was identical to the free phase at the same P, T [65, 66]. Excess sorption is easier to measure unambiguously, but it requires the input of the pore volume [67-69]. In simulations, bulk fluid density and fugacities are obtained from biased test insertions in the NPT ensemble of the free gas. Pore volume is determined by simulated helium pycnometry in the same organic solid. Then, total sorption is obtained from GCMC simulations, and excess sorption is determined by subtracting the mass of bulk fluid that would be contained in the pore volume. In Figure 16, we show that the total sorption in the micropores of the kerogen model from Grand Canonical simulation increases continuously with increasing pressure. The excess sorption is displaying a maximum for pressures in the order of 10 MPa at 338 K. The explanation is that the adsorption capacity is already saturated when the bulk fluid has still a low density. Further increase in pressure will increase the density of the bulk fluid without increasing so much the adsorbed amount, thus explaining the decrease in excess sorption. The influence of temperature has been investigated in the interval 323-353 K: the amount of excess sorption decreases when temperature increases, but the shape of the excess sorption isotherm is unchanged. This is consistent with experimental measurements [70]. Qualitatively, the maximum excess sorption of methane has been observed in studies on dried gas shales by Gasparik *et al.* [71], as is shown in the right hand side of Figure 16; in their work, maxima in the excess isotherms were observed for all but the least-mature sample. However, it is possible that the adsorption on gas shales is more complex than adsorption on kerogen, as the clay minerals present a significant surface area in these samples.

Only a qualitative and maybe a semi-quantitative comparison of our simulation results and the experimental findings (that are presented in *Fig. 16*) is meaningful, due to several facts:

– our simulation model was built upon average composition and structural information provided by experimental studies as has already been discussed and was not intended to represent any particular kerogen system and specifically the kerogens that are experimentally studied and presented in Figure 16;
– in this study, we have used a microporous kerogen model (*i.e.* pores with a pore width that is less than 2 nm). For a quantitative description of the system, mesopores should also be considered (pore width in

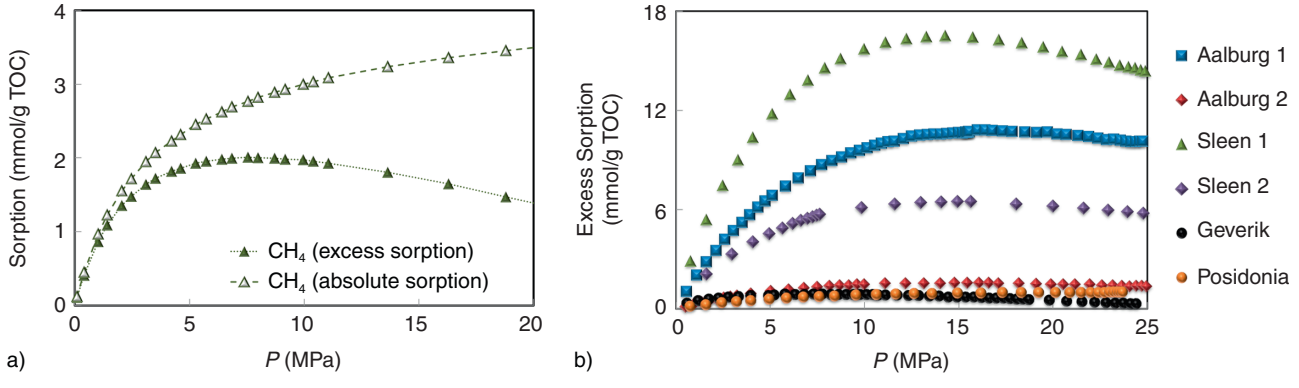

Figure 16

a) Methane adsorption isotherms (excess and absolute sorption isotherms) obtained *via* molecular simulation on the mature kerogen model of Figure 15. Sorption is indicated here in millimoles of gas per gram of Total Organic Carbon (TOC). b) Excess sorption isotherms for methane (mmol·g^{-1} of TOC *vs* MPa) measured on dry samples at 338 K from experimental study of Gasparik *et al.* [71].

the range of 2 to 50 nm), along with the interfaces of organic and inorganic matter;
- adsorption isotherms obtained by Monte-Carlo simulations provide what should be considered an upper limit of the loading onto the solid. Kinetic constraints, such as the possible obstruction of molecule movement due to the presence of other molecules that are more strongly interacting with the solid (such as water) or the existence of close pores which are not accessible by the sorbed molecules, cannot be taken into account in GCMC simulations, as the introduction of molecules into the system is done by creating and destroying molecules at randomly selected places in the solid based on the system's energy, without considering how the molecules should reach that location;
- interface phenomena (between the organic and inorganic phases of the solid) may play an important role on the adsorption and diffusion of pure compounds and especially of mixtures in the organic phase. Those phenomena should be accounted for, either explicitly or effectively, in order first to assess their significance and then take their effect under consideration, if there is a need to;
- the anisotropy of stress on such systems in reservoir conditions is not considered in our simulations, nor is it in most of the experimental studies. Scarce experimental findings in literature do not help in building appropriate models or comparing with simulation results. Swellings of charcoal, kerogen and coal upon gas adsorption have been reported in the literature [72] but the difficulty of measuring swelling and adsorption simultaneously is prohibiting the existence of many public datasets on this topic. At the same time, this is an area where simulation could be used to shed some light in the driving forces for swelling and the mechanisms involved.

Among other features, Grand Canonical simulation may be used to implement a test of hydrophobicity for a given microporous material from its adsorption isotherm [73].
- when water sorption is low for fugacity values lower than the saturated vapor pressure of water, and increases for higher fugacities, the material is hydrophobic. This means that high intrusion pressures of liquid water are needed to fill the pores;
- when water sorption capacity is saturated before the fugacity reaches the vapor pressure of water at the same temperature, the material is either hydrophilic or mixed hydrophilic/hydrophobic.

As mentioned in the literature, these systems display sometimes hysteresis when simulating adsorption + desorption paths by Grand canonical simulations. A hydrophobicity study has been carried out on both ideal and non-ideal slit pore models of kerogen and coal. The various models used in this hydrophobicity study were not identical to the model available from reference [74]. That model was rather the starting point and the reference that was used for comparing all different models. The inner surface of the pores was changed in each model by introducing different polar groups, which can be found in coal as well as "holes" in the graphene layer facing inside the pore. This rather systematic study has not been aiming at creating realistic pore surfaces, but rather at mimicking the crude effect that introducing "defects" on the ideal graphene surface would have. The model in reference [74] has been used as a reference and comparison because it has been built to simulate a specific material. It showed a good agreement when comparing simulation results against experimental data. The number of graphene layers and the distance of these layers, in all our models, are been set in agreement with the model of reference [74]. Various pore widths have been used for all different models. In a systematic sensitivity study, the following features were found:
- when the material does not contain polar groups (hydroxyl, pyrrole) facing micropores, kerogen and coal internal surfaces are hydrophobic;
- when the material contains few polar groups accessible on the walls of micropores, the material is hydrophilic, a liquid-like water phase anchoring to the hydroxyl groups.

The interpretation is that polar groups form hydrogen bonds with water molecules, making water condensation more favorable in micropores.

The kerogen model has been also used to investigate the co-adsorption of CO_2 and water as a function of CO_2 fugacity. In pores of 1.0 nm diameter such as sketched in Figure 14, several tens of water molecules may condense in a small droplet with a structure comparable to liquid water (*Fig. 17*). In very small pores, *i.e.* ultramicropores (below 0.5 nm) the width of the pore is insufficient for water molecules to self-organize in a three-dimensional liquid-like droplet. However this behavior is found for low CO_2 fugacity only. When CO_2 fugacity increases, the micropore is no more filled with a liquid-like water phase but with a dense CO_2 phase.

In the process of organic maturation with increasing burial, a progressive loss of hydroxyl groups and other polar groups is observed [75]. It is thus expected that kerogen progressively changes from hydrophilic (or partly hydrophilic) to hydrophobic when maturation proceeds. When a gas shale or a coal sample is moisture-equilibrated, water droplets may significantly decrease the available pore volume and hamper the transport of gas molecules. This is a possible cause of the very

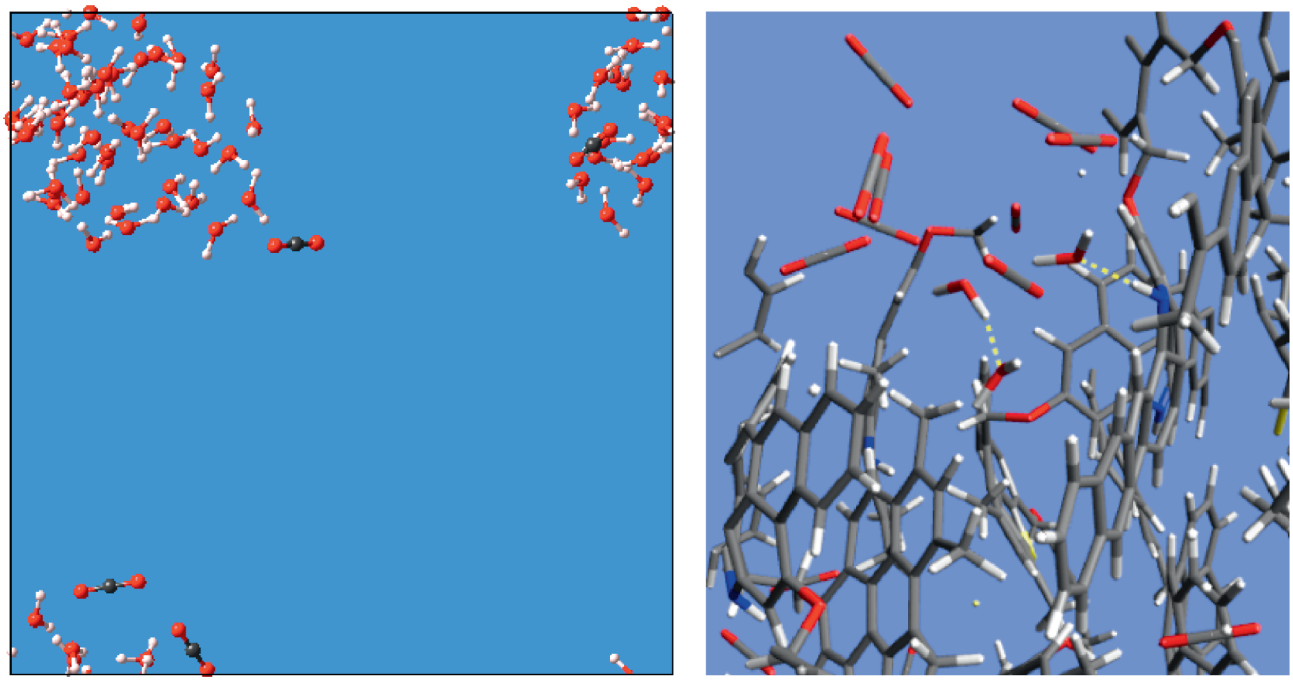

Figure 17

Binary mixture of CO_2 and H_2O in kerogen. a) Only the adsorbed molecules are displayed, at fugacities, $f_{CO_2} = 0.4$ MPa and $f_{H_2O} = 0.018$ MPa; b) adsorbed molecules along with the kerogen structure (a small portion of the simulation box is displayed including part of the pore and part of the kerogen matrix), at $f_{CO_2} = 1.0$ MPa and $f_{H_2O} = 0.018$ MPa. Hydrogen bonds are displayed as yellow dotted lines.

different shape of methane adsorption isotherms in dry and moist conditions.

Another experimental observation that is explained by molecular modeling is the difference in initial slope between the adsorption isotherms of helium, argon, methane, and ethane [2]. It was found that this sequence is essentially explained by the increase of the interaction energy of guest molecules with the kerogen framework.

Although still preliminary, such explanations illustrate the strength of molecular modeling in understanding complex systems in conditions where experiments are difficult.

CONCLUSIONS - PERSPECTIVES

The examples shown in this article illustrate the unique capabilities of molecular simulations to treat realistic systems, either with zeolites, carbon nanotubes or naturally occurring materials like coal or kerogen. It is highly satisfactory that hexane/benzene selectivity inversions between silicalite and faujasites are well predicted with published forcefields. Also, the satisfactory description of adsorption isotherms, for light gases or ethane-thiol, illustrate the capacity of molecular modeling to capture most of the relevant parameters in the adsorption on crystalline microporous adsorbents. The coupling of *ab-initio* and Grand Canonical Monte Carlo methods will certainly increase the reliability of predictions when polar fluids are considered [37].

Concerning kerogen, it is highly encouraging that models of kerogen can be built in agreement with known chemistry of these systems. Obtaining realistic densities with the very simple relaxation approach considered here is also encouraging for the investigation of other kerogen types or of various maturity levels. Moreover, computing excess sorption curves in qualitative agreement with those recently measured on dry samples of gas shale are a very good point for molecular modeling.

Among the problems that are not yet captured by GCMC simulation, swelling upon adsorption of microporous materials is certainly a fascinating challenge. Deformation of the adsorbent is common in a large range of materials. Swelling of polymeric systems upon adsorption [76, 77], coal swelling induced by gas adsorption [72], behavior of clay minerals [78, 79], or cement paste [80] are some examples of deformations of porous materials on which performing reliable simulations remains challenging in the perspective of industrial applications. There has been recent progress in this field, by introducing the Osmotic Framework Adsorbed

Solution Theory (OFAST) [81] and by performing simulations in the osmotic ensemble [82]. There is still a promising development to be done, in order to establish an efficient process of dealing with a wide range of systems, combining existing methodologies and expanding them to treat complex systems.

ACKNOWLEDGMENTS

We are indebted to *Total SA* for support to part of the work presented here. Guillaume Galliero and Julien Collell (University of Pau) are acknowledged for fruitful discussions. We thank B. Krooss (*RWTH Aachen*), Benoit Coasne for stimulating discussions and advice. GIBBS license from: IFP Energies nouvelles and Laboratoire de Chimie-Physique, Université de Paris-Sud, CNRS.

REFERENCES

1 Ruthven D.M. (1984) *Principles of adsorption and adsorption processes*, Wiley, New York.

2 Schettler P.D., Parmely C.R. (1989) *SPE Reserv. Eng. J.* **1**, 283-287.

3 Pollastro R.M., Jarvie D.M., Hill R.J., Adams C.W. (2007) *AAPG Bull.* **91**, 4, 405-437.

4 Nicholson D., Parsonage N.G. (1982) *Computer simulation and the statistical mechanics of adsorption*, Academic Press, New York, USA.

5 Plimpton S. (1995) *J. Comput. Phys.* **117**, 1-19.

6 Sun H., Mumby S.J., Maple J.R., Hagler A.T. (1994) *J. Am. Chem. Soc.* **116**, 2978.

7 Rigby D. (2010) Materials Design Inc., PCFF+. Refined PCFF forcefield parameters for aromatic and aliphatic compounds.

8 Jorgensen W.L., Maxwell D.S., Tirado-Rives J. (1996) *J. Am. Chem. Soc.* **118**, 11225.

9 Wick C.D., Stubbs J.M., Rai N., Siepmann J.I. (2005) *J. Phys. Chem. B* **109**, 40, 18974-18982.

10 Wick C.D., Martin M.G., Siepmann J.I. (2000) *J. Phys. Chem B* **104**, 8008.

11 Stubbs J.M., Potoff J.J., Siepmann J.I. (2004) *J. Phys. Chem. B* **108**, 17596-17605.

12 Stubbs J.M., Chen B., Potoff J.J., Siepmann I.J. (2001) *Fluid Phase Equilib.* **183-184**, 301-309.

13 Martin M.G., Siepmann J.I. (1998) *J. Phys. Chem. B* **102**, 2569.

14 Toxvaerd S. (1997) *J. Chem. Phys.* **107**, 5197.

15 Toxvaerd S. (1990) *J. Chem. Phys.* **93**, 4290.

16 Ahunbay M.G., Perez-Pellitero J., Contreras-Camacho R.O., Teuler J.M., Ungerer P., Mackie A.D., Lachet V. (2005) *J. Phys. Chem. B* **109**, 2970-2976.

17 Bourasseau E., Haboudou M., Boutin A., Fuchs A.H., Ungerer P. (2003) *J. Chem. Phys.* **118**, 3020-3034.

18 Bourasseau E., Ungerer P., Boutin A. (2002) *J. Phys. Chem. B* **106**, 5483-5491.

19 Bourasseau E., Ungerer P., Boutin A., Fuchs A.H. (2002) *Molec. Simul.* **28**, 317-336.

20 Contreras-Camacho O., Ungerer P., Boutin A., Mackie A. D. (2004) *J. Phys. Chem. B* **108**, 14109-14114.

21 Delhommelle J., Tschirwitz C., Ungerer P., Granucci G., Millié P., Pattou D., Fuchs A.H. (2000) *J. Phys. Chem. B* **104**, 4745-4753.

22 Perez-Pellitero J., Bourasseau E., Demachy I., Ridard J., Ungerer P., Mackie A. (2008) *J. Phys. Chem. B* **112**, 32, 9853-9863.

23 Perez-Pellitero J., Ungerer P., Mackie A.D. (2007) *J. Phys. Chem. B* **111**, 17, 4460-4466.

24 Ungerer P., Beauvais C., Delhommelle J., Boutin A., Rousseau B., Fuchs A.H. (2000) *J. Chem. Phys.* **112**, 5499-5510.

25 Buttefey S., Boutin A., Fuchs A.H. (2002) *Molec. Simul.* **28**, 1049.

26 Beauvais C., Guerrault X., Coudert F.-X., Boutin A., Fuchs A.H. (2004) *J. Phys. Chem. B* **108**, 399-404.

27 Smit B. (1995) *Mol. Phys.* **85**, 153.

28 dePablo J.J., Laso M., Suter U.W. (1992) *J. Chem. Phys.* **96**, 6157.

29 Maginn E.J., Bell A.T., Theodorou D.N. (1995) *J. Phys. Chem.* **99**, 2057.

30 Dodd L.R., Boone T.D., Theodorou D.N. (1993) *Molec. Phys.* **78**, 961-996.

31 Allen M.P., Tildesley D.J. (1987) *Computer simulation of liquids*, Oxford Science Publications, Oxford.

32 Frenkel D., Smit B. (1996) *Understanding Molecular Simulation*, Academic Press, San Diego.

33 Macedonia M.D., Maginn E.J. (1999) *Molec. Phys.* **96**, 1375-1390.

34 Errington J.R., Panagiotopoulos A.Z. (1999) *J. Chem. Phys.* **111**, 9731.

35 Uytterhoven L., Dompas D., Mortier W.J. (1992) *J. Chem. Soc. Faraday Trans.* **88**, 2753-2760.

36 Mortier W.J., Ghosh S.K., Shankar S. (1986) *J. Am. Chem. Soc.* **108**, 4315-4320.

37 Rozanska X., Ungerer P., Leblanc B., Yiannourakou M. (2013) *Oil Gas Sci. Technol. – Rev. IFP Energies nouvelles*, **68** (2) 299-307.

38 Cracknell R.F., Nicholson D., Parsonage N.G. (1990) *Molec. Phys.* **71**, 931.

39 Widom B. (1963) *J. Chem. Phys.* **39**, 2808-2812.

40 Ungerer P., Tavitian B., Boutin A. (2005) *Applications of molecular simulation in the oil and gas industry - Monte-Carlo methods*, Editions Technip, Paris.

41 Burgess C.G.V., Everett D., Nuttall D. (1989) *Pure Appl. Chem.* **61**, 11, 1845-1852.

42 Ravikovitch P.I., Neimark A.V. (2001) *Colloids Surfaces, A. Physicochem. Eng. Aspects* **187-188**, 11-21.

43 Neimark A.V., Ravikovitch P.I., Vishnyakov A. (2002) *Phys. Rev. E* **65**, 3, 031505.

44 Puibasset J. (2009) *Langmuir* **25**, 903-911.

45 Jeffroy M., Boutin A., Fuchs A.H. (2011) *J. Phys Chem. B* **115**, 15059–15066.

46 Watanabe T., Manz T.A., Sholl D.S. (2011) *J. Phys. Chem. C* **115**, 4824-4836.

47 Wender A., Barreau A., Lefebvre C., DiLella A., Boutin A., Ungerer P., Fuchs A.H. (2006) *Adsorp. Sci. Technol.* **24**, 8, 713.

48 Pérez-Pellitero J., Amrouche H., Siperstein Flor R., Pirngruber G., Nieto-Draghi C., Chaplais G., Simon-Masseron A., Bazer-Bachi D., Peralta D., Bats N. (2010) *Chem. Eur. J.* **16**, 1560-1571.

49 Jaramillo E., Auerbach S.M. (1999) *J. Phys. Chem. B* **103**, 9589-9594.

50 Buttefey S., Boutin A., Mellot-Draznieks C., Fuchs A. (2001) *J. Phys. Chem. B* **105**, 9569-9575.

51 Du Z., Vlugt T.J.H., Smit B., Manos G. (1998) *AIChE J.* **44**, 1756-1764.

52 Pascual P., Pernot P., Ungerer P., Tavitian B., Boutin A. (2003) *Phys. Chem. Chem. Phys.* **5**, 3684.

53 Leroy F., Rousseau B. (2004) *Molec. Simul.* **30**, 9, 617-620.

54 Sun M.S., Talu O., Shah D.B. (1996) *J. Phys. Chem.* **100**, 17276.

55 Sun M.S., Shah D.B., Xu H.H., Talu O. (1998) *J. Phys. Chem. B* **102**, 1466.

56 Abdul-Rehman H.B., Hasanain N.A., Loughlin K.F. (1990) *Ind. Eng. Chem. Res.* **29**, 1525-1535.

57 Yu M., Hunter J.T., Falconer J.L., Noble R.D. (2006) *Micropor. Mesopor. Mater.* **96**, 376-385.

58 Weber G., Benoit F., Bellat J.-P., Paulin C., Mougin P., Thomas M. (2008) *Microporous and Mesoporous Materials*, **109**, 184-192.

59 Kelemen S.R., Afeworki M., Gorbaty M.L., Sansone M., Kwiatek P.J., Walters C.C., Freund H., Siskin M., Bence A.E., Curry D.J., Solum M., Pugmire R.J., Vandenbroucke M., Leblond M., Behar F. (2007) *Energy & Fuels* **21**, 3, 1548-1561.

60 Oberlin A., Boulmier J.L., Villey M. (1980) in *Kerogen, Insoluble Organic Matter from Sedimentary Rocks*, Durand B.E. (ed), Editions Technip, Paris, pp. 191-241.

61 Okiongbo K.S., Aplin A.C., Larter S.R. (2005) *Energy & Fuels* **19**, 6, 2495-2499.

62 Van Krevelen D.W. (1993) *Coal - Typology - Physics - Chemistry – Constitution*, 2nd ed, Elsevier.

63 Zhang L., Greenfield M. (2007) *Energy & Fuels* **21**, 1102-1111.

64 Sondergeld C.H., Newsham K.E., Comisky J.T., Rice M.C., Rai C.S. (2010) Petrophysical Considerations in Evaluating and Producing Shale Gas Resources, in *SPE Unconventional Gas Conference*, Pittsburgh, Pennsylvania, 23-25 Feb, *SPE paper* 131768.

65 Sircar S. (2001) *AIChE J.* **47**, 1169.

66 Krooss B.M., Van Bergen F., Gensterblum Y., Siemons N., Pagnier H.J.M., David P. (2002) *Int. J. Coal Geol.* **51**, 2, 69-92.

67 Gensterblum Y., Van Hemert P., Billemont P., Busch A., Charrière D., Lia D., Krooss B.M., de Weireld G., Prinz D., Wolf K.-H.A.A. (2009) *Carbon* **47**, 2958-2969.

68 Gensterblum Y., Van Hemert P., Billemont P., Battistutta E., Busch A., Krooss B.M., De Weireld G., Wolf K.-H.A. A. (2010) *Int. J. Coal Geol.* **84**, 115-124.

69 Busch A., Gensterblum Y., Krooss B.M., Siemons N. (2006) *Int. J. Coal Geol.* **66**, 53-68.

70 Gasparik M., Ghanizadeh A., Gensterblum Y., Krooss B., Littke R. (2012) presented at the *3rd EAGE Shale workshop - Shale Physics and Shale Chemistry*, Barcelona, Spain, 25 Jan, (unpublished).

71 Gasparik M., Ghanizadeh A., Bertier P., Gensterblum Y., Bouw S., Krooss B.M. (2012) *Energy Fuels* **26**, 8, 4995-5004.

72 Vandamme M., Brochard L., Lecampion B., Coussy O. (2010) *J. Mech. Phys. Solids* **58**, 10, 1489-1505.

73 Desbiens N., Demachy I., Fuchs A.H., Kirsch-Rodeschini H., Soulard M., Patarin J. (2005) *Angewandte Chemie* **117**, 5444-5447.

74 Billemont P., Coasne B., De Weireld G. (2010) *Langmuir* **27**, 3, 1015-1024.

75 Tissot B.P., Welte D.H. (1984) *Petroleum Formation and Occurrence*, Springer, Berlin.

76 Faure F., Rousseau B., Lachet V., Ungerer P. (2007) *Fluid Phase Equilib.* **261**, 1-2, 168-175.

77 Escobedo F.A., dePablo J.J. (1999) *J. Chem. Phys.* **110**, 1290.

78 Rotenberg B., Marry V., Dufrêche J.-F., Malikova N., Giffaut E., Turq P. (2007) *Comptes Rendus Chimie* **10**, 10-11, 1108-1116.

79 Malikova N., Cadéne A., Marry V., Dubois E., Turq P., Zanotti J.-M., Longeville S. (2005) *Chem. Phys.* **317**, 226-235.

80 Pellenq R.J.-M., Kushima A., Shahsavari R., Van Vliet K.J., Buehler M.J., Yip S., Ulm F.J. (2009) *Proceedings of the National Academy of Sciences* **106** 38, 16102-16107.

81 Coudert F.-X., Mellot-Draznieks C., Fuchs A.H., Boutin A. (2009) *J. Am. Chem. Soc. Commun.* **131**, 3442-3443.

82 Coudert F.-X., Boutin A., Jeffroy M., Mellot-Draznieks C., Fuchs A.H. (2011) *Chem. Phys. Chem.* **12**, 2, 247-258.

Manuscript accepted in February 2013
Published online in November 2013